Supporting Information for

Switchable Luminescent Probe for Trace-Level Detection of Spodoptera Litura Nuclear Polyhedrosis Virus via Color-Changing Response

Dipen Biswakarma, [a,c] ‡ Nilanjan Dey,[a] ‡ Deepa Bhagat,[d] Santanu Bhattacharya*,[a,b,c]

[a]Department of Organic Chemistry, Indian Institute of Science, Bangalore 560012, India

[b]School of Applied & Interdisciplinary Sciences, Indian Association for the Cultivation of Science, Jadavpur, Kolkata 700032, India

[c]Jawaharlal Nehru Centre for Advanced Scientific Research, Jakkur, Bengaluru 560064, Karnataka, India

[d]National Bureau of Agriculturally Insect Resources, P.B. No. 2491, H. A. Farm Post, Bangalore 560 024, India

Table of Contents

General Synthetic Scheme:

Synthetic Scheme 1:

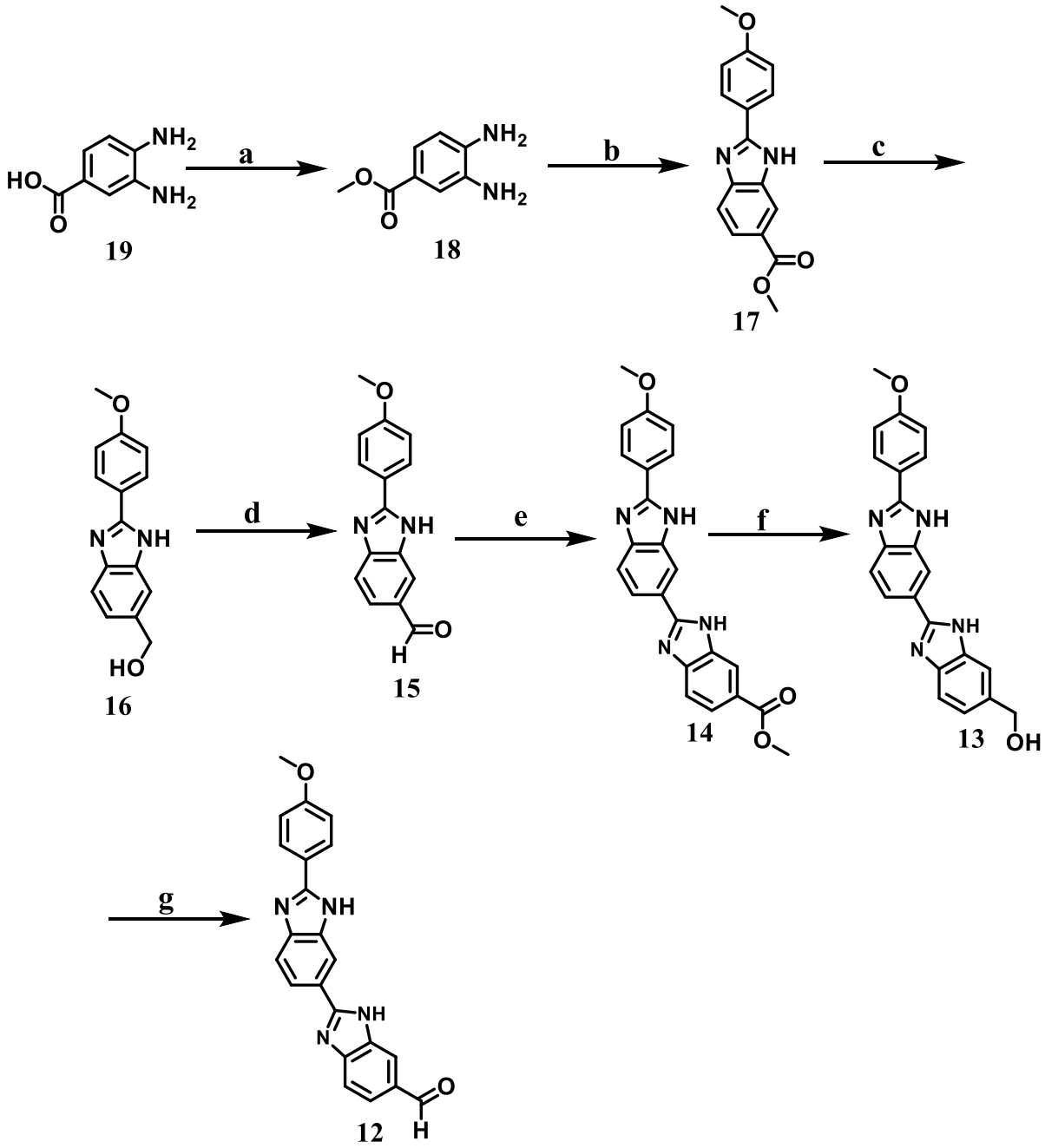

Reagents, Conditions and Yields: (a) MeOH, Conc. H_2SO_4, Reflux, 24 h, 96%. (b) p- anisaldehyde, $Na_2S_2O_5$, EtOH, reflux, 24 h, 70 %; (c) LAH, THF, rt, 15 h, 65 %; (d) PCC, THF, rt, 10 h; (e) **18**, $Na_2S_2O_5$, EtOH, reflux, 24 h, 70 %; (f) LAH, THF, rt, 15 h, 65 %; (g) PCC, THF, rt, 10 h.

Synthetic Scheme 2:

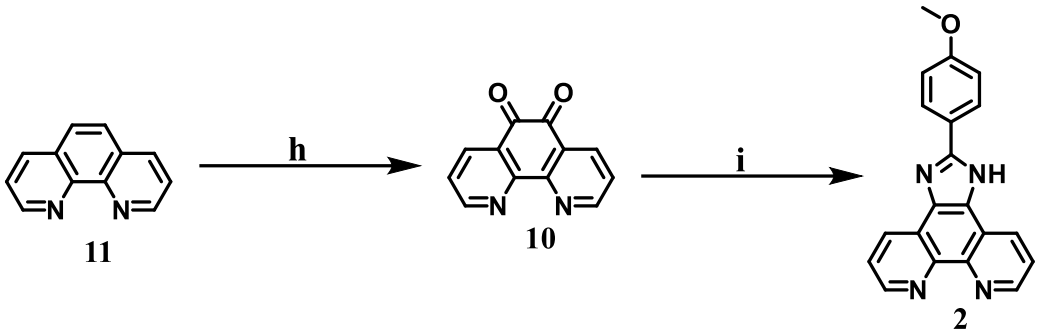

Reagents, Conditions and Yields: (h) Conc. H_2SO_4, Conc. HNO_3, KBr, 0 ^oC-Reflux, 3 h, 95%; (i) p-anisaldehyde, NH_4Ac, Glacial AcOH, Reflux, 6 h, 80%.

Synthetic Scheme 3:

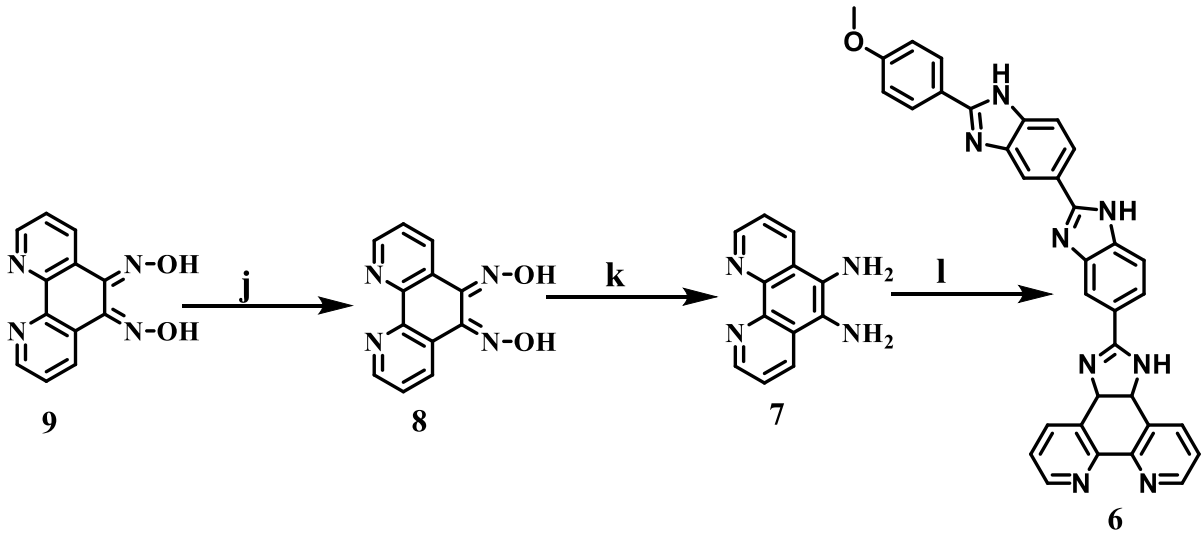

Reagents, Conditions and Yields: (j) $NH_2OH.HCl$, Na_2CO_3, EtOH, reflux, 5h; (k) H_2, Pd/C (10 %), EtOH, rt, 24 h, 89 %; (l) **12**, $Na_2S_2O_5$, EtOH, reflux, 24 h, 60 %.

Synthetic Scheme 4:

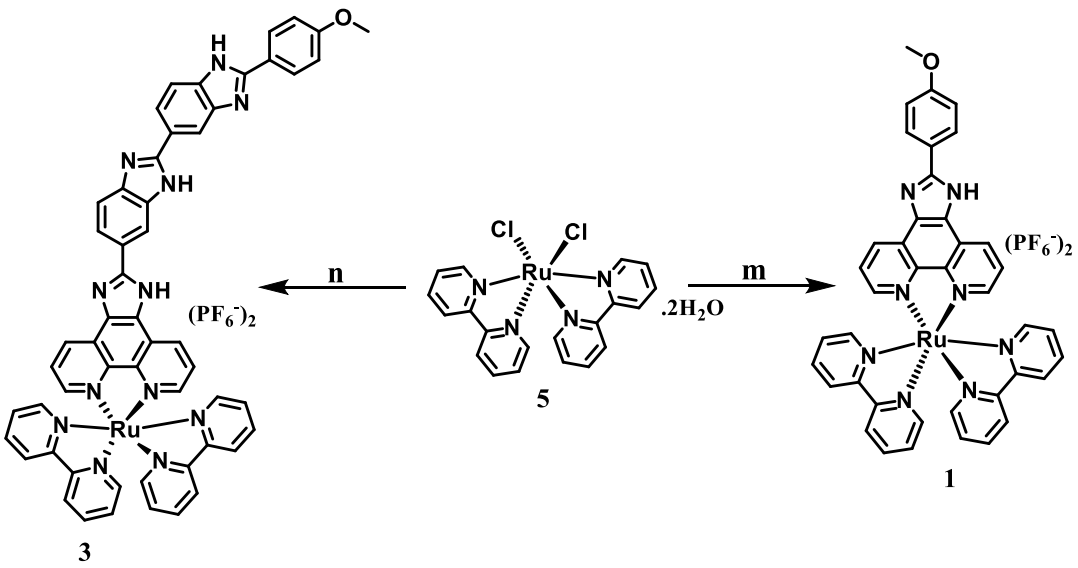

Reagents, Conditions and Yields: (m) **2**, MeOH: H_2O (1:1), reflux, 12 h, NH_4PF_6, 68%. (n) **6**, MeOH: H_2O (1:1), reflux, 12 h, NH_4PF_6, 55%.

Synthesis and characterisation

Compound **1**, **2**, **3** and **4** were synthesized using procedure reported in the literature. [S1-S3]

Characterization of compound 1. Yield: 73%; FT-IR (KBr): 3356, 1593, 840 cm^{-1}; ^1H NMR (DMSO-d_6, 400 MHz) δ ppm 3.73 (s, 3H), 7.35 (m, 2H), 7.45(m, 2H), 7.85 (d, *J* = 7.8 Hz, 2H), 7.90 (m, 2H), 8.02 (d, *J* = 7.6 Hz, 2H), 8.10 (t, *J* = 8.4 Hz, 2H), 8.21 (t, *J* = 7.6 Hz, 4H), 8.85 (m, 4H), 9.08 (d, *J* = 8Hz, 2H); ^{13}C NMR (DMSO-d_6, 100 MHz): 55.70, 112.30, 114.60, 119.85, 121.30, 122.50, 124.0, 124.32, 125.23, 126.89, 130.50, 132.75, 136.98, 139.68, 148.75, 150.12, 152.32, 157.65, 157.70, 158.23, 161.23; HRMS : m/z found 884.10 $[M\text{-}PF_6^-]^+$, 738.4 $[M\text{-}2PF_6^-H]+$, 370.2 $[M^{+2}/2]$, 1029 calcd. Elem. Anal.: Calc. for $C_{40}H_{34}F_{12}N_8O_3P_2Ru$: C: 45.08; H: 3.22; N: 10.51. Found: C: 45.05; H; 3.21; N; 10.52.

Characterization of compound 2: Yield:73%; ^1H NMR (DMSO-d_6, 400 MHz) δ ppm 3.73 (s, 3H), 7.41 (d, *J* = 7.8 Hz, 2H), 7.82 (m, 2H), 8.21 (d, *J* = 8Hz, 4H), 8.95 (d, *J* = 8Hz, 2H), 9.03 (d, *J* = 8Hz,

2H); HRMS for $C_{20}H_{14}N_4O$: m/z found 327.26 [M-H] +, calcd. 327.12; Elem. Anal.: calcd. for $C_{20}H_{14}N_4O$ C, 69.8; H, 4.68; N, 16.3; Found: C, 69.39; H, 4.65; N, 16.24.

Characterization of compound 3. Yield: 42 %; FT-IR (KBr): 3370, 1590, 838 cm^{-1}; ^1H NMR (DMSO-d_6, 400 MHz) δ ppm 3.87 (s, 3H), 7.14 (d, *J* = 7.8 Hz, 2H), 7.57 (d, *J* = 7.6 Hz, 2H), 7.59 (m, 4H), 7.66, (d, *J* = 7.8 Hz, 1H), 7.71 (d, 1H), 7.83 (s, 1H), 7.84 (s, 1H), 7.90 (m, 2H), 8.07 (d, *J* = 7.6 Hz, 1H), 8.10 (t, *J* = 8.4 Hz, 2H), 8.17 (d, *J* = 7.6 Hz, 2H), 8.18 (s, 1H), 8.21 (t, 4H), 8.37 (s, 1H), 8.48 (d, 2H), 8.85 (m, 4H), 9.09 (d, *J* = 8 Hz, 2H); HRMS: m/z found 1117 $[M\text{-}PF_6^-]^+$, 971 $[M\text{-}2PF_6^-\text{-}H]+$, 631 $[M^{+2}/2]$, 1261.98 calcd. Elem. Anal.: Calc. for $C_{54}H_{42}F_{12}N_{12}O_3P_2Ru$: C: 49.97; H: 3.26; N: 12.95. Found: C: 49.95; H; 3.27; N; 12.94.

References:

S1. Mandal, S.; Poria, D. K.; Ghosh, R.; Ray, P. S.; Gupta, P. Development of a cyclometalated iridium complex with specific intramolecular hydrogen-bonding that acts as a fluorescent marker for the endoplasmic reticulum and causes photoinduced cell death. *Dalton Trans.* **2014**, *43*, 17463-17474.

S2. Shi, S.; Liu, J.; Li, J.; Zheng, K. C.; Huang, X. M.; Tan, C. P.; Chen, L. M.; Jia, L. N. Synthesis, characterization and DNA-binding of novel chiral complexes Δ- and Λ-[Ru(bpy)2L]2+ (L = o-mopip and p-mopip). *J. Inorg. Biochem.* **2006**, *100*, 385-395.

S3. Friedman, A. E.; Chambron, J. C.; Sauvage, J. P; Turro, N. J.; Barton J. K. Molecular "Light Switch" for DNA: $Ru(bpy)_2(dppz)^{2+}$. *J. Am. Chem. Soc.* **1990**, *112*, 4960-4962.

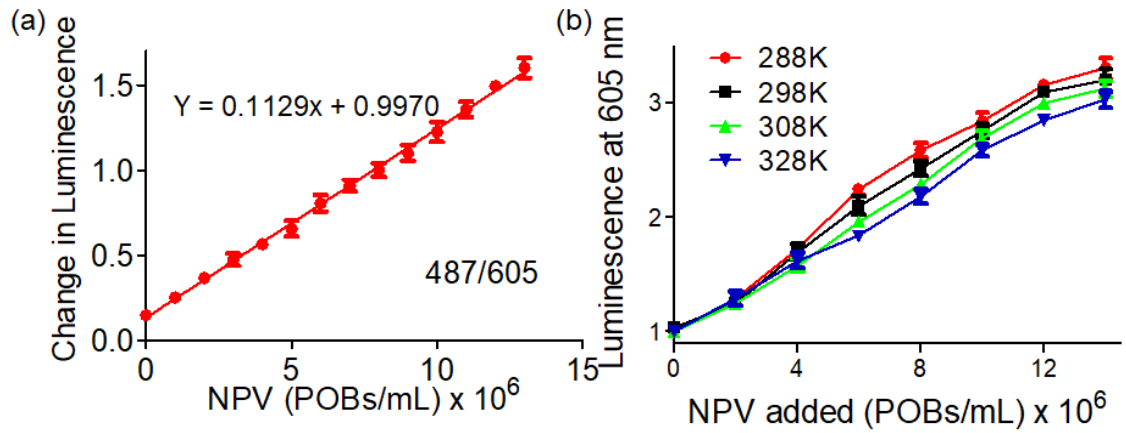

Figure S1. (a) Change in the luminescence of **1** (10 μM, λ_{ex} = 450 nm) at I_{487} /I_{605} upon gradual addition of SLNPV in water (pH 7.4) (no of independent experiment: 3). (b) Effect of temperature on the interaction of **1** (10 μM, λ_{ex} = 450 nm) with SLNPV (1.4 × 10^7 POBs/mL) in water at pH 7.4 monitored at 605 nm (no of independent experiment: 3).

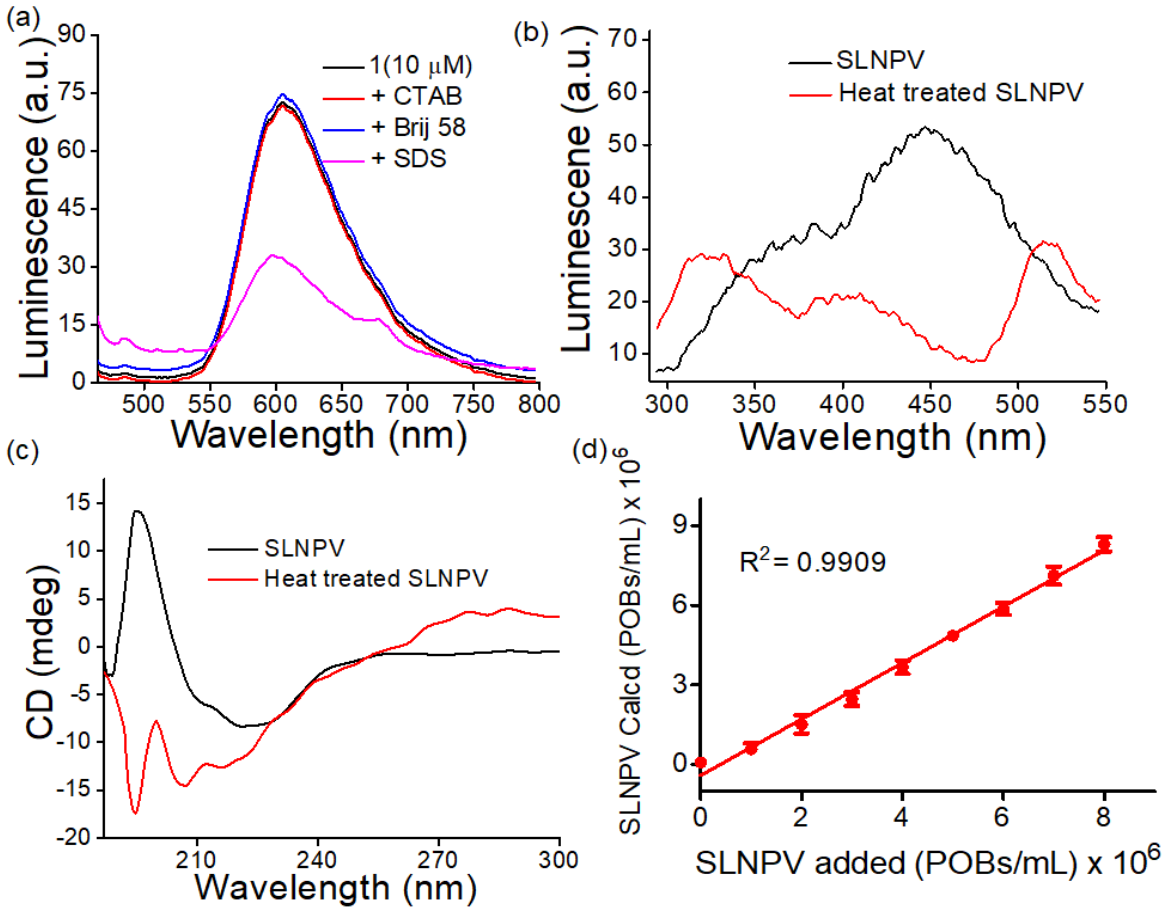

Figure S2. (a) Change in luminescence of **1** (10 μM, λ_{ex} = 450 nm) in the presence of surfactant CTAB (1 mM), Brij 58 (1 mM) and SDS (8 mM) at pH 7.4 in water. Heat induced change in (b) luminescence (λ_{ex} = 280 nm), (c) CD spectra of SLNPV at pH 7.4 in water. (d) Recovery plot shows quantitative estimation of SLNPV in spodomar® extract using **1** (10 μM) at pH 7.4 in water (no of independent experiment: 3).

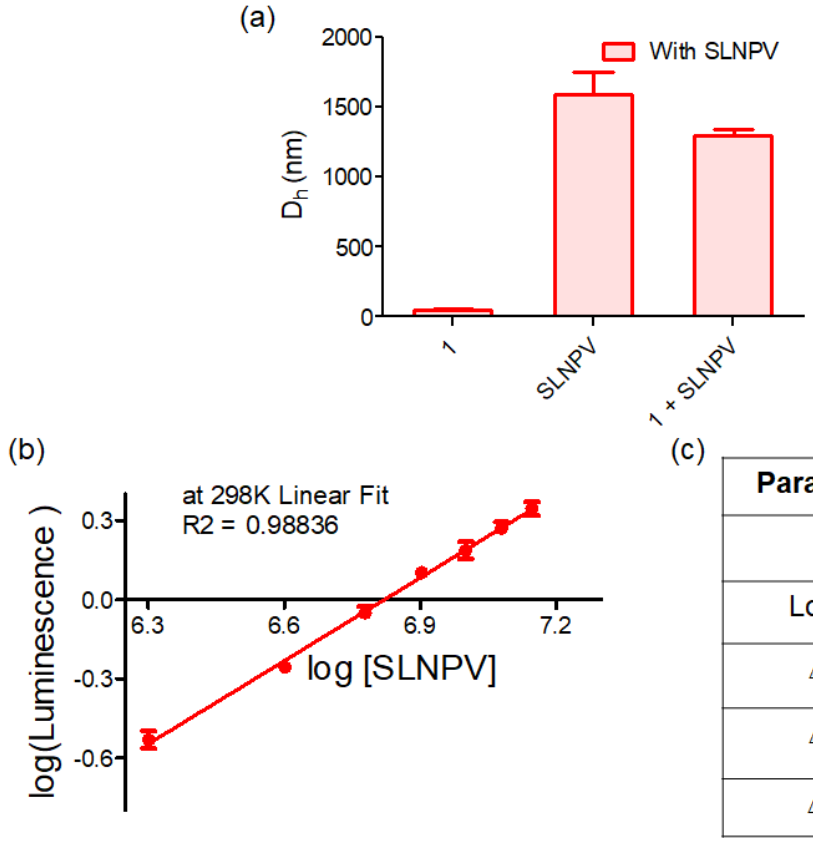

(c)

Parameter	Value
T	298 K
Log K	-8.198
ΔH	-2.85 KJ/ mol
ΔS	0.0179 J/ mol
ΔG	-8.20 KJ/mol

Figure S3. (a) Change in hydrodynamic diameter of compound **1** (10 μM, λ_{ex} = 450 nm) in the presence of SLNPV at pH 7.4 in water (no of independent experiment: 3). (b, c) Determination of various thermodynamic parameters associated with interaction of **1** with SLNPV at pH 7.4 in water (at 298 K) (no of independent experiment: 3).

Discussion on excitation spectral analysis: It is known in the literature that dual mode emission from Ru (II) complex is generally originated from ligand-to-ligand charge-transfer (LLCT, at higher energy region) and MLCT (at low energy region) transitions. The absorptions between 300 and 400 nm are mainly responsible for the higher-energy emission, while the lower-energy emission is associated with UV and visible region spanning from 400 to 600 nm. As a result, two emission bands show different excitation spectra. Thus, by examining the nature of the excitation spectra, we can claim that emission at 605 nm is primarily originated from MLCT transition, whereas the luminescence band at 487 nm is predominantly attributed to LLCT transition.

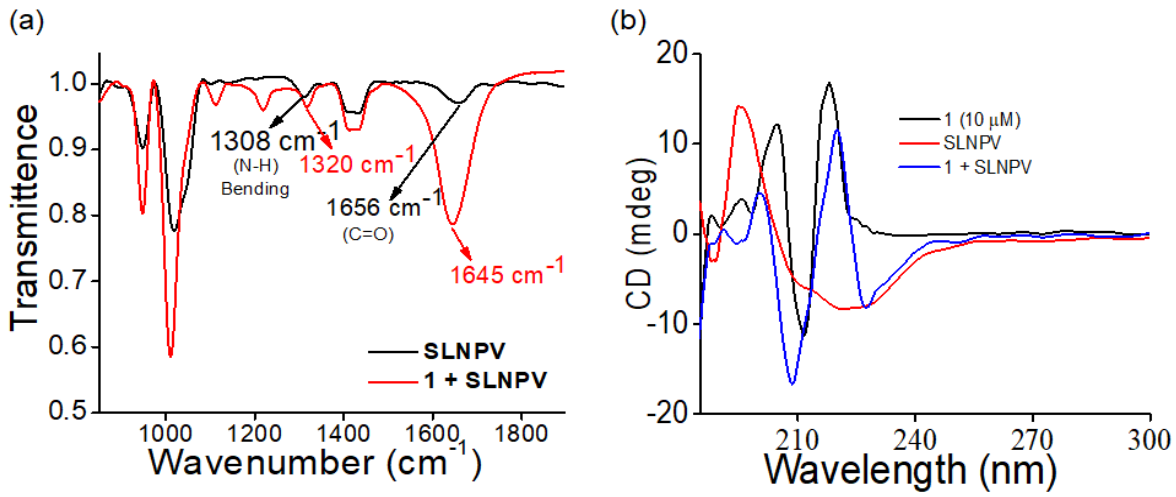

Figure S4. (a) FT-IR spectra of SLNPV (1.3×10^7 POBs/mL) in the presence and absence of compound **1** (50 μM) at pH 7.4 in water. (b) CD spectra of **1** (10 μM) in the presence and absence of SLNPV (1.3×10^7 POBs/mL).

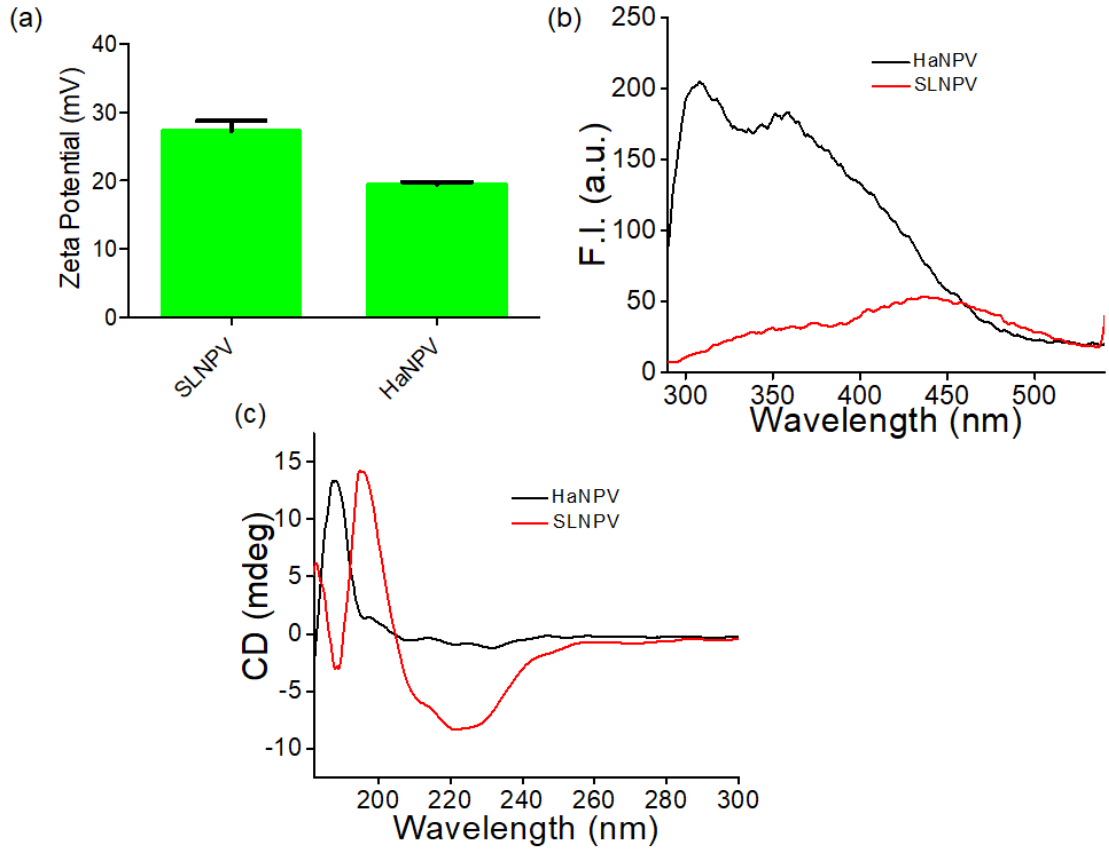

Figure S5. (a) Zeta potential of SLNPV and HaNPV (10 μM) at pH 7.4 in water (no of independent experiment: 3). (b) Fluorescence spectra (λ_{ex} = 280 nm) and (c) CD spectra of SLNPV and HaNPV (1.3×10^7 POBs/mL) at pH 7.4 in water.

Discussion: The emission spectrum of SLNPV (λ_{ex} = 280 nm) was found to have a red-shifted emission maximum with relatively less emission intensity in comparison to HaNPV (Figure S5b). This suggests that the tyrosine and tryptophan moiety present in the SLNPV are in a relatively polar environment (solvent-exposed) than that of HaNPV. CD spectral analysis also confirms that the tertiary structures of the outer protein layer are sufficiently different for HaNPV and SLNPV. The α-helical pattern was more prominent in the case of SLNPV (Figure S5c). The superior binding affinity of **1** towards SLNPV might be contributed by the combination of the factors described above. Nevertheless, such differentiation is crucial since the host plants for *H. Armigera* (curable by HaNPV treatment) are not the same as that of *S. Litura* (curable by SLNPV treatment). Thus, the agriculture crops which require spraying of SLNPV will not be benefitted if charged with HaNPV.

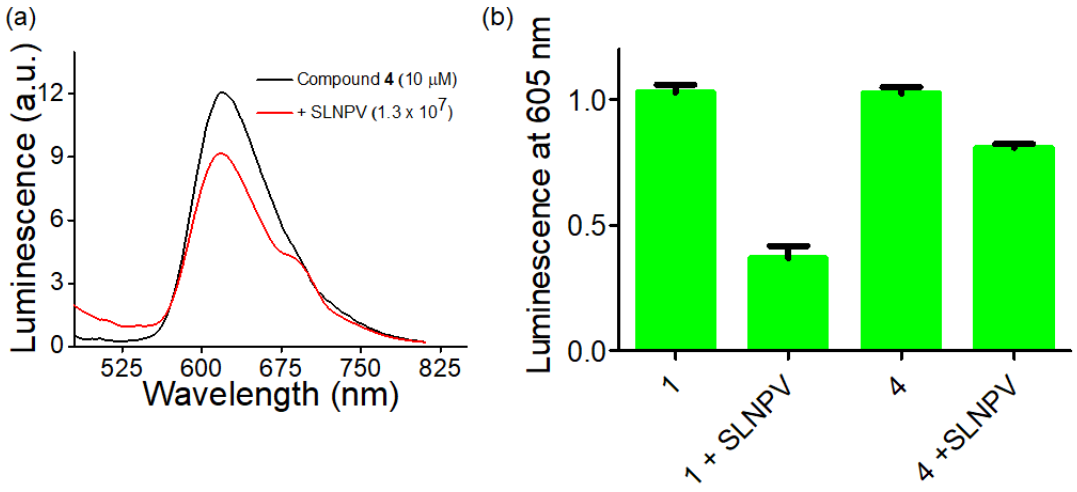

Figure S6. (a) Luminescence spectra (λ_{ex} = 460 nm) of **4** (10 μM) in the presence of SLNPV (1.3 × 10^7 POBs/mL) at pH 7.4 in water. (b) Comparison plot for the interaction of compound **1** and **4** with SLNPV (1.3 × 10^7 POBs/mL) at pH 7.4 in water (no of independent experiment: 3).

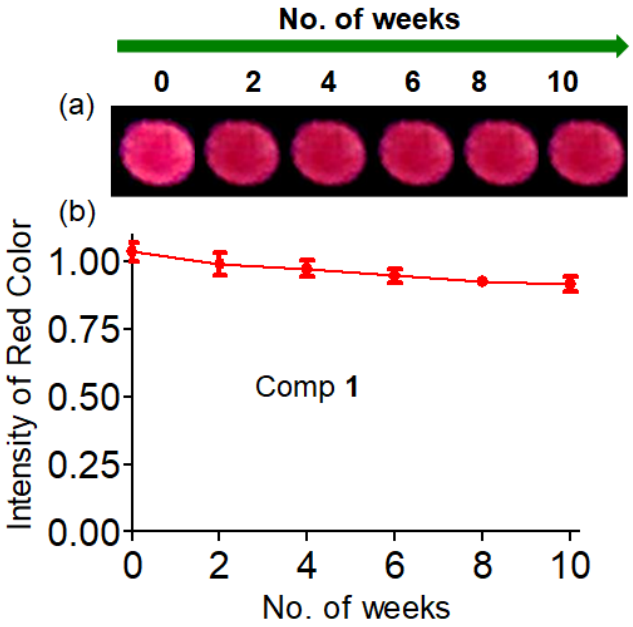

Figure S7. (a) Images captured (under 365 nm UV lamp) after addition of SLNPV onto the precoated paper discs of **1**. (b) Changes in red luminescence of paper strips at different time periods (no of independent experiment: 3).

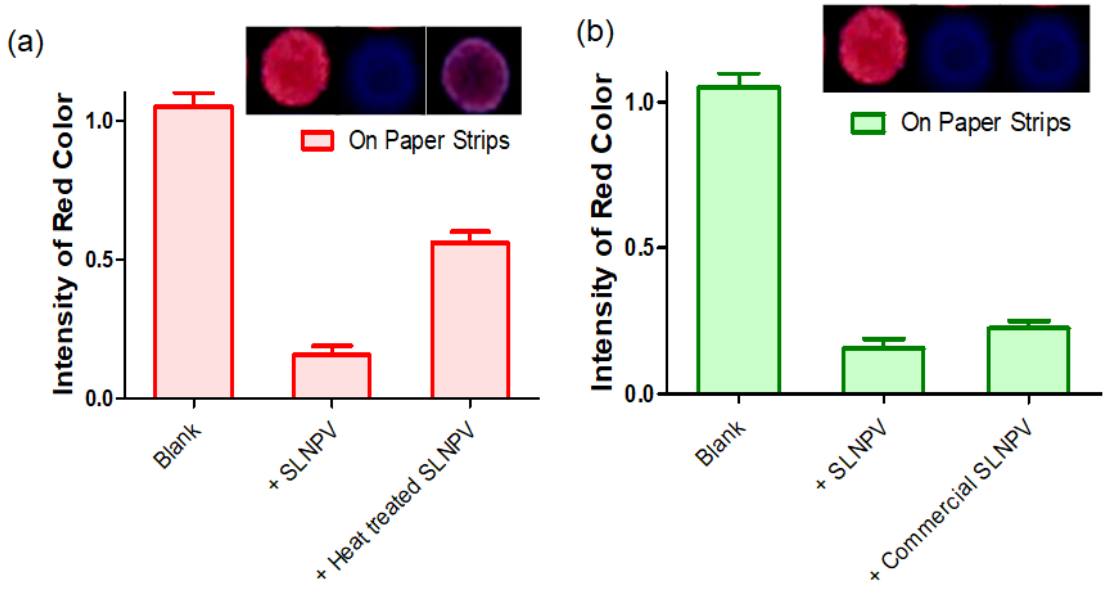

Figure S8. (a) Change in red color intensity of the precoated discs (with compound **1**) upon addition of both fresh and heat treated SLNPV (no of independent experiment: 3). (b) Change in red color intensity of the precoated discs (with compound **1**) upon addition of both pure and commercial mixture of SLNPV (no of independent experiment: 3).

Agricultural Crops	Detection Limit ($\times 10^3$ POBs/mL)	Agricultural Crops	Detection Limit ($\times 10^3$ POBs/mL)
Mango	6.03±0.02	Cotton	6.80±0.01
Orange	6.70±0.01	Amaranth	4.95±0.02
Apple	6.35±0.02	Sorghum	5.20±0.02
Strawberry	6.45±0.03	Sugar Cane	5.47±0.03
Papaya	5.47±0.01	Tomato	6.80±0.02
Banana	7.38±0.03	Egg Plant	6.25±0.01
Lettuce	5.82±0.02	Beans	5.30±0.03
Cabbage	6.10±0.03	Broccoli	6.05±0.02
Beet Root	5.78±0.01	Corn	6.94±0.01
Pea Nut	6.72±0.02	Ground Nut	6.34±0.01

Table S1. Estimation of minimum detectable concentration of SLNPV on interaction with compound **1** (10 μM) in different crop extracts at pH 7.4 in water.